Fast DOA Estimation in the Spectral Domain and Its Applications

Le Zuo[1, 2, *], Jin Pan[1], and Boyuan Ma[1]

Abstract—This paper presents a direction of arrival (DOA) estimation method. Spectral-domain interferometer equation is first established based on integral transforms of spatial interferometer equations. The direction finding problem in the spatial domain is thereby mapped to that in the spectral domain, relating angular parameters to spatial spectrums. This method is then applied to DOA estimation with circular arrays and spherical arrays. As a result, the elevation angle and azimuth angle are decoupled, giving closed-form and analytical formulae for DOA estimations by discrete phase samples on a sampling aperture. Algebraic relations between angular parameters and phase samples are established, and this method is hence computationally efficient. The Cramer-Rao lower bound (CRLB) of the proposed method is derived, and accuracy analysis demonstrates that the proposed method approaches the CRLB. In addition, mathematical insights into accuracy enhancement by large number of samples are observed via Parseval's theorem. Finally, numerical simulations and experimental measurements are provided to verify the effectiveness and appealing performance of the proposed method.

1. INTRODUCTION

Estimating two-dimensional (2-D) direction of arrival (DOA) of incident plane waves is important in array signal processing due to its applications in radar, sonar, and mobile communications [1]. Radio frequency DOA estimation is implemented by a direction finding (DF) array, involving multiple sensors placed at different positions in space to receive fields of a single incident wave or multiple incident waves arriving from different directions. For a single incident wave, phase interferometers are commonly employed, which utilize measured phase differences across the array to estimate DOAs [2]. Array configurations and the associated DOA algorithms are closely related to DF accuracy and efficiency. Regarding to array configurations, a linear array (LA) was first studied, which provides a one-dimensional (1-D) source bearing angle relative to the array axis [3]. Then a rectangular array (RA) emerged to extend the LA when 2-D DOA is needed [4–8]. DOA estimations using LA and RA interferometers are based on analytical and accurate functions relating phase differences to angular parameters. Therefore, the calculation is computationally efficient. Nevertheless, a circular array (CA) became the center of interest in the context of 2-D DOA estimation due to its attractive advantages of 360° azimuthal coverage, almost unchanged directional pattern and additional elevation angle information [1, 9, 10]. The dominant methods in analyzing CAs are by means of the so-called phase-mode excitation, which is essentially the decomposition of the array excitation function into different Fourier harmonics by using Fourier analysis. It comes from the fact that the beam pattern of a CA is periodic in azimuth [11–14].

However, for a CA the source elevation cannot be estimated with the same accuracy as the azimuth angle because of CAs' planar structure. Moreover, a 180° ambiguity typically appears in the elevation angle, since the azimuth plane is often a symmetrical plane for the array geometry. A spherical array

* Corresponding author: Le Zuo (zorro1204@163.com).
[1] University of Electronic Science and Technology of China, Chengdu, China. [2] Nanyang Technological University, Singapore.

(SA), where the sampling elements are distributed over a sphere, overcomes these disadvantages. A spatially symmetrical spherical array can offer high estimation accuracies for both the elevation and azimuth plane [15]. With the development of SAs, many existing algorithms were reformulated using spherical harmonics (SHs) [16, 17] as counterparts to Fourier harmonics for CAs. A wide variety of DOA estimation algorithms have been proposed employing SHs [18–27]. Most of these compute a metric over a dense azimuth-inclination grid before identifying its peak(s) as the DOA(s) [23]. Generally, these algorithms are based on the phase mode of receiving complex responses and require a sufficiently large number of elements to avoid spatial aliasing. Moreover, although this method exhibits good performance, it is associated with significant computational burden due to the eigenvalue decomposition of a complex covariance matrix and the 2-D peak search as a whole, thus the computational load is still significant [25].

The problem of reducing the computational complexity by using simple formulations has attracted substantial attention. Decoupling two bearing angles is attractive, since it can relax computational complexity. The UCA-RARE algorithm for CAs [26, 27] and a two-stage method for SAs [15] were developed since they decouple the estimation of the azimuth angle from the estimation of the elevation angle. However, due to a residual error, these methods introduce errors in form of bias and excess variance and hence, the obtained estimates may be far from optimal, especially when the number of sensors is small [14]. Accordingly, to avoid biased estimation and complex computation, an unbiased DOA estimation method for CA and SA interferometers is developed in this paper. The method is based on the spectral-domain interferometer equation (SDIE), which transforms the DF problem from the spatial domain to its corresponding spectral domain by integral transforms. The underlying DOA estimation problem is then reformulated as an equivalent spectrum extraction problem in the spectral domain via integral transforms of phase data on a sampling aperture. When it is applied to CA and SA interferometers, the two angular parameters, i.e., the azimuth and elevation angles, are decoupled and an analytical solution to 2-D DOA is thereafter obtained from phase samples of an incident plane wave. In addition, the proposed method only requires algebraic operations. The estimation accuracy is further explained by Parseval's theorem in the context of spectral domain, which enables us to develop some mathematical insights into how the element number of a DF array affects the estimation accuracy. Accuracy analysis is devised by the benchmark evaluation of the Cramer-Rao lower bound (CRLB). The results demonstrate that the proposed method attains the CRLBs for both CAs and SAs, and hence it is an optimal estimation method. Finally, numerical examples and experimental measurements are provided to verify the proposed method.

The proposed method differs from the existing ones mainly in that it decomposes phases of incident fields rather than complex values of fields. The main contribution of this paper is to present such a strategy of analysis that wave functions are exploited to expand the phase distribution of the incoming wave. Furthermore, algebraic relations between angular parameters and DOA-related spectrums are established, and consequently, the algorithm is computationally efficient and accurate in that it provides algebraic and exact formulations for 2-D DOA estimation. The major advantages of the strategy are the resultant analytical formulations, reduced element number requirement, unbiased estimation, and computational efficiency.

The rest of the paper is organized as follows. Section 2 establishes the interferometer equation in the spatial domain. In Section 3, the IE is transformed into the spectral domain. The DOA-related spectrum calculation is developed in Section 4. Section 5 addresses accuracy analysis of the method. Simulation and measurement results are presented in Section 6 and Section 7, respectively. Section 8 concludes this paper.

2. INTERFEROMETER EQUATION IN THE SPATIAL DOMAIN

For a single incident wave from the far-field with elevation angel θ_s and azimuth angle φ_s, where the elevation angle $\theta_s \in [0, \pi)$ is measured down from the z axis, and the azimuth angle $\varphi_s \in [0, 2\pi)$ is measured counterclockwise from the x axis, the phase of the electric field is expressed as

$$\Phi = \mathbf{k} \cdot \mathbf{r} \tag{1}$$

where $\mathbf{k}$ is the wave vector, represented by $\mathbf{k} = k(\sin\theta_s \cos\varphi_s \hat{a}_x + \sin\theta_s \sin\varphi_s \hat{a}_y + \cos\theta_s \hat{a}_z)$, with $k = 2\pi/\lambda$ the wave number in free space, λ the wavelength of the incident wave, and $\hat{a}_x$, $\hat{a}_y$, $\hat{a}_z$ unit

vectors of x, y, z axis, respectively.

An interferometer is a receiving system composed of elements located at $\mathbf{r}$, which adopts the sampled phases of electric fields to determine the DOA of an incident wave. The phase distribution and 2-D DOA satisfy the following interferometer equation (IE),

$$\Phi = \Phi\left(\mathbf{r}; \theta_s, \varphi_s\right). \tag{2}$$

In the IE, the bearing angles are manifested in the wave vector, and the resultant phase distribution is determined by the projection of the wave vector, i.e., $\mathbf{k}$, onto the position vector, i.e., $\mathbf{r}$. For a circular aperture with a radius of ρ_0 in the xoy-plane, as shown in Fig. 1, the spatial distribution of the phase of the incoming wave can be expressed as

$$\Phi_{CA}\left(\mathbf{r}; \theta_s, \varphi_s\right) = k\rho_0 \sin\theta_s \cos\left(\varphi_s - \varphi\right) + \Phi_0 \tag{3}$$

where Φ_0 is the initial phase of the incoming wave, which can also be interpreted as the phase of the incident wave arriving at the center of the array. Meanwhile, for a spherical aperture with a radius of r_0 centered at the origin of the spherical coordinate, as shown in Fig. 2, the spatial distribution of the phase of the incoming wave is represented by

$$\Phi_{SA}\left(\mathbf{r}; \theta_s, \varphi_s\right) = kr_0 \sin\theta \sin\theta_s \cos\left(\varphi_s - \varphi\right) + kr_0 \cos\theta \cos\theta_s + \Phi_0. \tag{4}$$

It is worth noting that Eqs. (3) and (4) are systems of transcendental equations about θ_s and φ_s, in which the two unknowns are coupled, and hence not analytical. Therefore, we expect to develop an accurate and efficient solution to these equations.
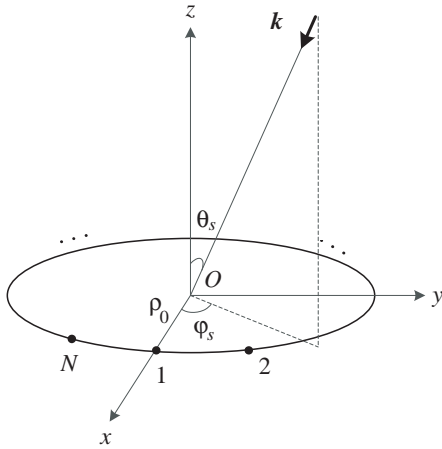

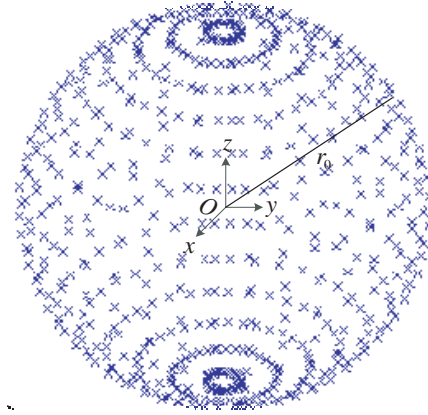**Figure 1.** Geometry of a circular aperture.

Figure 2. Geometry of a spherical aperture.

3. SPECTRAL-DOMAIN INTERFEROMETER EQUATION

The main strategy of the spectral-domain interferometer equation (SDIE) is patterned on the integral transform of Eq. (1), which transforms the DF problem in the spatial domain to that in its corresponding spectral domain, expecting to get a simple and analytical solution to the angular parameters. The general formation of an integral transform is given by

$$\Psi\left(\boldsymbol{\lambda}; \theta_s, \varphi_s\right) = \int \Phi\left(\mathbf{r}; \theta_s, \varphi_s\right) t\left(\mathbf{r}, \boldsymbol{\lambda}\right) d\mathbf{r} \tag{5}$$

where $\boldsymbol{\lambda} = (\lambda_1, \lambda_2, \lambda_3)$ is the spectral variable, and $t(\mathbf{r}, \boldsymbol{\lambda})$ is the kernel of the integral transform, which can be derived from the eigen-functions of wave equations under various coordinates. The dependence of θ_s and φ_s on $\mathbf{r}$ in the spatial domain is transformed to the dependence on $\boldsymbol{\lambda}$ in the spectral domain. Therefore, Eq. (5) is termed spectral-domain interferometer equation (SDIE). For convenience of notation, we will drop the explicit dependence of θ_s and φ_s in the following.

Electromagnetic waves in free space satisfy scalar Helmholtz equations in homogeneous media [28], i.e.,

$$\nabla^2 \psi + k^2 \psi = 0 \tag{6}$$

where ψ denotes a scalar potential. Wave functions are canonical solutions to Helmholtz equations under different coordinates and form complete sets that can be used as bases to expand general solutions of Helmholtz equations. In the Cartesian coordinate, eigen-functions of wave equations are in the form of $\exp(j\boldsymbol{\lambda} \cdot \mathbf{r})$, where $j = \sqrt{-1}$, which makes the integral in Eq. (5) the Fourier transform. Thus, the DOA estimation in the spatial domain is transformed to the spectral domain, i.e., the Fourier domain, resulting in the solution to the IE in the spectrum of the Fourier transform, and yielding

$$\Psi(\boldsymbol{\lambda}) = \int \Phi(\mathbf{r}) \exp(j\boldsymbol{\lambda} \cdot \mathbf{r}) d\mathbf{r}. \tag{7}$$

Given a planar array at $z = 0$ that samples the phase distribution of $\Phi(\mathbf{r})|_{z=0}$, the SDIE of which can be obtained from Eq. (7) and yields

$$\Psi(\boldsymbol{\lambda}) = 2\pi \delta(\lambda_3) \int_{-\infty}^{+\infty} \int_{-\infty}^{+\infty} \Phi(\mathbf{r})|_{z=0} \exp(j\lambda_1 x + j\lambda_2 y) \, dx dy. \tag{8}$$

where $\delta(\lambda_3)$ is an impulse function. Since the DOA estimation utilizing phases is irrelevant of the coefficient, the SDIE of planar arrays is then the 2-D Fourier transform of the IE in the spatial domain and is given by

$$\Psi(\lambda_1, \lambda_2) = \int_{-\infty}^{+\infty} \int_{-\infty}^{+\infty} \Phi(\mathbf{r})|_{z=0} \exp(j\lambda_1 x + j\lambda_2 y) \, dx dy. \tag{9}$$

The three-dimensional (3-D) SDIE can be obtained similarly in various coordinates with corresponding kernels of integrals. In the spherical coordinate, the SDIE is given by

$$\Psi(m, n, \lambda) = \int_0^{+\infty} \int_0^{2\pi} \int_0^{\pi} \Phi(\mathbf{r}) \, j_n(\lambda r) \, P_n^m(\cos\theta) \exp(jm\varphi) \sin\theta \, d\theta d\varphi dr \tag{10}$$

where $P_n^m(\cos\theta)$ denotes the associate Legendre function of degree m and order n, $j_n(\lambda r)$ denotes the spherical Bessel function of order n of first kind. The 2-D spherical SDIE can be set up as an alternative of Eq. (10), i.e., sampling the phase distribution of $\Phi(\mathbf{r})|_{r=r_0}$ gives

$$\Psi(m, n) = \int_0^{2\pi} \int_0^{\pi} \Phi(\mathbf{r}) \, P_n^m(\cos\theta) \exp(jm\varphi) \sin\theta \, d\theta d\varphi dr. \tag{11}$$

Similarly, the 3-D SDIE in the cylindrical coordinate is given by

$$\Psi(n, \lambda_1, \lambda_2) = \int_0^{2\pi} \int_{-\infty}^{+\infty} \int_0^{+\infty} \Phi(\mathbf{r}) \, J_n(\lambda_2 \rho) \exp(jn\varphi) \exp(j\lambda_1 z) \, d\rho dz d\varphi \tag{12}$$

where $J_n(\lambda_2 \rho)$ denotes the Bessel function of order n of first kind. Sampling the phase distribution of $\Phi(\mathbf{r})|_{\rho=\rho_0}$ gives the 2-D cylindrical SDIE, namely

$$\Psi(n, \lambda_1) = \int_{-\infty}^{+\infty} \int_0^{2\pi} \Phi(\mathbf{r})|_{\rho=\rho_0} \exp(jn\varphi) \exp(j\lambda_1 z) \, d\varphi dz. \tag{13}$$

Furthermore, sampling the phase distribution of $\Phi(\mathbf{r})|_{\rho=\rho_0, z=0}$ gives the 1-D circular SDIE

$$\Psi(n) = \int_0^{2\pi} \Phi(\mathbf{r})|_{\rho=\rho_0, z=0} \exp(jn\varphi) \, d\varphi, \tag{14}$$

which is also recognized as the 1-D Fourier transform. Taking Eq. (3) into Eq. (14) leads to the analytic expression of the SDIE for a CA, namely

$$\Psi_{CA}(n) = \pi k \rho_0 \sin\theta_s \left(\delta[n-1] \exp(j\varphi_s) + \delta[n+1] \exp(-j\varphi_s)\right) + 2\pi \Phi_0 \delta[n] \tag{15}$$

where $\delta[n]$ is a Kronecker delta function. Finally, the SDIE for a CA is obtained, in which the two angular parameters are contained in the spectrum of 1 and -1. According to the symmetry property

of Fourier transform, $\Psi_{CA}(1) = \Psi_{CA}^*(-1)$, where $*$ denotes complex conjugate, i.e., the two points in the spectral domain contain the same information about the DOA, and $\Psi_{CA}(1)$ gives the 2-D DOA, namely

$$\Psi_{CA}(1) = \pi k \rho_0 \sin \theta_s \exp(j\varphi_s). \tag{16}$$

Note that in Eq. (16) the two angular parameters, i.e., θ_s and φ_s, are decoupled in the spectrum of 1, depending on the magnitude and the phase of $\Psi_{CA}(1)$, respectively, namely

$$\theta_s = \sin^{-1}(|\Psi_{CA}(1)|/(\pi k \rho_0)), \tag{17}$$
$$\varphi_s = \arg(\Psi_{CA}(1)), \tag{18}$$

where $\arg(x)$ is the argument of x, which signifies that θ_s and φ_s can be extracted through the acquisition of phases around a circular aperture.

For a CA, the eigen function is the 1-D Fourier transform, while for a SA, the eigen function is Legendre function and Fourier function. With regards to a SA, substituting Eq. (4) into Eq. (11) leads to the analytic expression of the SDIE for a SA, namely

$$\Psi_{SA}(0,0) = \int_0^{2\pi} \int_0^\pi \Phi_{SA}(\mathbf{r}) P_0^0(\cos\theta) \sin\theta d\theta d\varphi = 4\pi^2 \Phi_0, \tag{19}$$

$$\Psi_{SA}(0,1) = \int_0^{2\pi} \int_0^\pi \Phi_{SA}(\mathbf{r}) P_1^0(\cos\theta) \sin\theta d\theta d\varphi = 4\pi k r_0 \cos\theta_s/3, \tag{20}$$

$$\Psi_{SA}(1,1) = \int_0^{2\pi} \int_0^\pi \Phi_{SA}(\mathbf{r}) P_1^1(\cos\theta) \exp(j\varphi) \sin\theta d\theta d\varphi = 2\pi k r_0 \sin\theta_s \exp(j\varphi_s)/3. \tag{21}$$

Observe that the azimuth angle can be extracted from $\Psi_{SA}(1,1)$, while the elevation angle can be decoupled from the manipulations of $\Psi_{SA}(0,1)$ and $\Psi_{SA}(1,1)$, namely

$$\theta_s = \tan^{-1}(2|\Psi_{SA}(1,1)|/\Psi_{SA}(1,0)), \tag{22}$$
$$\varphi_s = \arg(\Psi_{SA}(1,1)). \tag{23}$$

Note that in these DOA estimation formulae based on the SDIE, two angular parameters are decoupled, resulting in a simple and compact solution to 2-D DOA. Moreover, acquisition of informative spectrums by sensor displacement can provide 2-D DOA estimations.

4. SPECTRUM CALCULATION

For applications, it is necessary to sample a continuous aperture at discrete positions [16]. The DOA information is contained in the spectrums, which can be calculated through the orthogonality of eigen functions. Orthogonality connotes the notation of perpendicularity between vectors. Since the wave functions are orthogonal, evaluating each spectrum is based on the projection of phase samples onto its corresponding wave functions.

4.1. Circular Array

According to Eq. (15), the discrete phase samples on the circumference of a circular aperture can be rewritten as

$$\Phi_i = k\rho_0 \sin\theta_s \cos(\varphi_s - \varphi_i) + \Phi_0 = \Psi_{CA}(-1)\exp(j\varphi_i) + \Psi_{CA}(1)\exp(-j\varphi_i) + \Psi_{CA}(0). \tag{24}$$

Each spectrum can be extracted by the inner product of the corresponding basis function. When $N \geq 3$, the orthogonal property of 1-D Fourier transform is represented by

$$\langle \exp(jl\varphi_i), \exp(jk\varphi_i) \rangle = \frac{1}{2\pi} \sum_{i=1}^N \exp(jl\varphi_i) \exp(jk\varphi_i) = \delta(l-k). \tag{25}$$

It is followed by the inner product of the discrete Fourier harmonicas on both sides of Eq. (24) that

$$\frac{1}{2\pi} \sum_{i=1}^N \Phi_i \exp(j\varphi_i) = \Psi_{CA}(1). \tag{26}$$

The other two spectrums vanish because of the orthogonal property of eigen functions.

Finally, considering Eqs. (17) and (18), the analytic and explicit formulae for the two angular parameters based on a CA are derived, namely

$$\hat{\theta}_s = \sin^{-1}\left(2\left|\sum_{i=1}^{N}\Phi_i \exp\left(j\varphi_i\right)\right| \middle/ \left(Nk\rho_0\right)\right), \tag{27}$$

$$\hat{\varphi}_s = \arg\left(\sum_{i=1}^{N}\Phi_i \exp\left(j\varphi_i\right)\right). \tag{28}$$

4.2. Spherical Array

According to Eqs. (19)–(21), the discrete phase samples on a spherical aperture can be rewritten as

$$\begin{aligned}
\Phi_{il} &= kr_0 \sin\theta_l \sin\theta_s \cos\left(\varphi_s - \varphi_i\right) + kr_0 \cos\theta_l \cos\theta_s + \Phi_0 \\
&= \Psi_{SA}\left(1,1\right)P_1^1\left(\cos\theta_l\right)\exp\left(j\varphi_i\right) + \Psi_{SA}\left(-1,1\right)P_1^{-1}\left(\cos\theta_l\right)\exp\left(-j\varphi_i\right) \\
&\quad + \Psi_{SA}\left(0,1\right)P_1^0\left(\cos\theta_l\right) + \Psi_{SA}\left(0,0\right)P_0^0\left(\cos\theta_l\right)
\end{aligned} \tag{29}$$

where $\varphi_i = 2\pi(i-1)/N$, $\theta_l = \pi(l-0.5)/M$, $i = 1,2,...,N$, $l = 1,2,...,M$ [29, 30]. The orthogonal property of associated Legendre functions and Fourier functions is represented by

$$\left\langle P_p^k\left(\cos\theta_l\right)\exp\left(jk\varphi_i\right), P_q^m\left(\cos\theta_l\right)\exp\left(jm\varphi_i\right)\right\rangle$$

$$= \sum_{l=1}^{M}\sum_{i=1}^{N}P_p^k\left(\cos\theta_n\right)\exp\left(jk\varphi_i\right)P_q^m\left(\cos\theta_l\right)\exp\left(-jm\varphi_i\right). \tag{30}$$

When $M \geq 2$ and $N \geq 3$, it holds that

$$\left\langle P_p^k\left(\cos\theta_l\right)\exp\left(jk\varphi_i\right), P_q^m\left(\cos\theta_l\right)\exp\left(jm\varphi_i\right)\right\rangle = \frac{4\pi}{2q+1}\frac{(q+m)!}{(q-m)!}\delta\left(k-m\right)\delta\left(p-q\right). \tag{31}$$

To extract $\Psi_{SA}(1,1)$, project phase samples onto $\{P_1^1(\cos\theta_l)\exp(\varphi_i)\}$, giving

$$\Psi_{SA}\left(1,1\right) = \sum_{l=1}^{M}\sum_{i=1}^{N}\Phi_{il}\sin\theta_l\exp\left(j\varphi_i\right)\Delta\theta\Delta\varphi \tag{32}$$

where $\Delta\theta = \pi/M$ and $\Delta\varphi = 2\pi/N$. Meanwhile, projection of phase samples onto $\{P_1^0(\cos\theta_l)\}$ leads to

$$\Psi_{SA}\left(0,1\right) = \sum_{l=1}^{M}\sum_{i=1}^{N}\Phi_{il}\cos\theta_l\Delta\theta\Delta\varphi. \tag{33}$$

Following Eqs. (32), (33), and combining Eqs. (22), (23), we obtain the algebraic formulae for 2-D DOA estimation based on the phase samples on a spherical aperture, namely

$$\hat{\theta}_s = \tan^{-1}\left(2\left|\sum_{l=1}^{M}\sum_{i=1}^{N}\Phi_{il}\sin\theta_l\exp\left(j\varphi_i\right)\right| \middle/ \sum_{l=1}^{M}\sum_{i=1}^{N}\Phi_{il}\cos\theta_l\right). \tag{34}$$

$$\hat{\varphi}_s = \arg\left(\sum_{l=1}^{M}\sum_{i=1}^{N}\Phi_{il}\sin\theta_l\exp\left(j\varphi_i\right)\right), \tag{35}$$

Note that Eqs. (27) and (28) have established algebraic relations between the DOA and discrete phase samples on the circumference of a circular aperture, while Eqs. (34) and (35) have established the algebraic relations between the DOA and the discrete phase samples on the periphery of a spherical aperture. In these formulations no approximations are made. It also worth noting that the minimum element number for a CA is three, and the minimum element number for a SA is three in the azimuth plane and two in the elevation plane. Even though a small number of elements is utilized, the estimation

is accurate, since there are no residual errors in neither phase distribution expansion nor spectrum computations. Besides, the initial phase Φ_0 is immaterial, as it does not appear in these estimation formulations and needs not even be known. Alternatively and conveniently, the phases can be measured with respect to any particular array element.

5. ACCURACY ANALYSIS

The SDIE implies that the computation of spectrums requires sampling phase data. However, in practice, some errors are expected in estimations, caused by several factors, such as thermal noises and hardware imperfections. The sampling errors will degrade spectrum calculation accuracy and hence DOA estimation accuracy.

5.1. Phase Extraction

As indicated in Eqs. (27), (28), (34), and (35), given the discretely sampled phases on an aperture, the 2-D DOA can be obtained without accuracy loss. In applications, the response observed at the receiver output is the exponent of phase distribution corrupted by additive white Gaussian noise (AWGN). The output of the ith element has the form $y_i(t) = A \exp(j\omega t + j\Phi_i) = n_i(t)$, where ω is the angular frequency, A is the magnitude of the signal, and $n_i(t)$ is an AWGN with zero mean and covariance σ_{noi}^2. The noises of each receiving channel are independent. The signal-to-noise ratio (SNR) is defined by $\mathrm{SNR} = A^2/\sigma_{noi}^2$.

The frequency of the signal is assumed to be accurately estimated using a number of well-known techniques [31]. The phase of each receiver output can be obtained by [32]

$$\tilde{\Phi}_i = \arg \left((1/M) \sum_{t=1}^{M} y_i(t) e^{-j\omega Tt} \right) \tag{36}$$

where T is the inverse of the constant sampling rate, and M is the number of snapshots. At moderately high SNR, an AWGN can be converted into an equivalent additive phase noise [33], i.e.,

$$\tilde{\Phi}_i = \arg(y_i) = \Phi_i + \xi_i \tag{37}$$

where ξ_i is the phase noise of the receiver, which is also Gaussian [33]. The variance of ξ_i is thus given by

$$\mathrm{var}(\xi_i) = 1/(2M\mathrm{SNR}). \tag{38}$$

Hence, the phase noise model reveals the interconnections between an AWGN and the phase sampling noise. Besides, since a typical implementation of a passive DF system involves a dedicated signal acquisition channel (receiver, analog-to-digital converter, etc.) for each sensor, phase measurement noises also arise from the presence of receiver noise, hardware imperfection, front end noise, etc. [34]. Then the phase samples can be written as $\tilde{\Phi}_i = \Phi_i + \varepsilon_i$, where ε_i is the overall phase noise on the ith receiving channel, which is assumed to be Gaussian with zero mean, σ^2 variance, and statistically independent [4], i.e.,

$$\mathrm{mean}(\varepsilon_i \varepsilon_l) = \sigma^2 \delta(i - l). \tag{39}$$

5.2. Bounds

In a measurement system, it is important to derive the best estimation that can be made with available observations. This section derives the CRLB in the absence of phase ambiguity, in order to demonstrate the potential predominance of the SDIE in the 2-D DOA estimation accuracy.

According to Eq. (24), the Jacobi matrix of DOA estimation using a CA is found by

$$\mathbf{J} = \begin{bmatrix} \frac{\partial \Phi_1}{\partial \theta_s} & \frac{\partial \Phi_1}{\partial \varphi_s} \\ \frac{\partial \Phi_2}{\partial \theta_s} & \frac{\partial \Phi_2}{\partial \varphi_s} \\ \vdots & \vdots \\ \frac{\partial \Phi_N}{\partial \theta_s} & \frac{\partial \Phi_N}{\partial \varphi_s} \end{bmatrix} = k\rho_0 \begin{bmatrix} \cos\theta_s \cos(\varphi_s - \varphi_1) & -\sin\theta_s \sin(\varphi_s - \varphi_1) \\ \cos\theta_s \cos(\varphi_s - \varphi_2) & -\sin\theta_s \sin(\varphi_s - \varphi_2) \\ \vdots & \vdots \\ \cos\theta_s \cos(\varphi_s - \varphi_N) & -\sin\theta_s \sin(\varphi_s - \varphi_N) \end{bmatrix}. \tag{40}$$

Hence, the Fisher information matrix (FIM) is given by [35]

$$\mathbf{F} = \frac{1}{\sigma^2}\mathbf{J}^T\mathbf{J} = \left[\begin{array}{cc} f_{11} & f_{12} \\ f_{21} & f_{22} \end{array} \right] \tag{41}$$

where $f_{11} = (k\rho_0\cos\theta_s/\sigma)^2\sum_{i=1}^{N}\cos^2(\varphi_s - \varphi_i) = N(k\rho_0\cos\theta_s)^2/(2\sigma^2)$, $f_{12} = f_{21} = -(k\rho_0/\sigma)^2\sin\theta_s\cos\theta_s\sum_{i=1}^{N}\cos(\varphi_s - \varphi_i)\sin(\varphi_s - \varphi_i) = 0$, $f_{22} = (k\rho_0\sin\theta_s/\sigma)^2\sum_{i=1}^{N}\sin^2(\varphi_s - \varphi_i) = N(k\rho_0\sin\theta_s)^2/(2\sigma^2)$. The CRLB is followed by the inverse of FIM, namely

$$\text{var}\,(\Delta\theta_s) \ \geq 2\sigma^2\,(k\rho_0\cos\theta_s)^{-2}\,/N, \tag{42}$$

$$\text{var}\,(\Delta\varphi_s) \ \geq 2\sigma^2\,(k\rho_0\sin\theta_s)^{-2}\,/N. \tag{43}$$

With regards to a SA, after considerable manipulations, the CRLB is evaluated by

$$\text{var}\,(\Delta\theta_s) \ \geq 4\sigma^2\,(kr_0)^{-2}\,\left(1 + \sin^2\theta_s\right)^{-1}/\,(MN)\,, \tag{44}$$

$$\text{var}\,(\Delta\varphi_s) \ \geq 4\sigma^2\,(kr_0\sin\theta_s)^{-2}\,/\,(MN)\,. \tag{45}$$

As indicated in Eqs. (42) and (43), the lower bounds of DOA estimation based on a CA are inversely proportional to the number of elements, and as the elevation angle increases, the accuracy of elevation angle estimation decreases, while the accuracy of azimuth angle estimation increases. It is worth mentioning that an inaccurate azimuth estimation is more important when the elevation angle is close to $90°$, compared to the azimuth estimation of a signal located near the pole of the sphere ($\theta_s = 0°$ or $180°$) [25]. As shown in Eq. (42), the accuracy of elevation estimation is inversely proportional to the cosine of the elevation angle, suggesting poor performance at the elevation angle of $90°$. This is clear because a planar array provides a larger aperture in the azimuth plane compared to the elevation plane. Comparing (44), the accuracy dependence on elevation angle is alleviated. It is also implied in Eqs. (42)–(45) that given a restricted aperture, one can increase element number to obtain high estimation accuracy.

5.3. Accuracy Analysis in the Spectral Domain

The algorithms exploit integral transforms, and therefore the accuracy of estimation should also be interpreted in the context of spectral domain. In the DOA estimation formulae, the underlying DOA estimation problem has been reformulated as an equivalent expansion coefficient extraction problem by discrete phase samples on the sampling aperture of a CA or a SA. The extraction of the angular parameters from the spectrums in the spectral domain is exact and hence accurate. Nevertheless, estimation errors arise from the inaccuracies of spectrum calculations. The spectrum calculations using noise-contaminated phases are evaluated as

$$\tilde{\Psi}(n) = \sum_{i=1}^{K}\tilde{\Phi}_i\psi_i^*(n) = \Psi(n) + \Delta\Psi(n) \tag{46}$$

where $K = N$ for a CA, $K = MN$ for a SA, and

$$\Psi(n) = \sum_{i=1}^{K}\Phi_i\psi_i^*(n), \tag{47}$$

$$\Delta\Psi(n) = \sum_{i=1}^{K}\varepsilon_i\psi_i^*(n). \tag{48}$$

Since $\psi_i^*(n)$ is a complete set of orthonormal basis functions, Parseval's theorem for a complete set of orthonormal basis functions relates the signal's energy to its expansion coefficients [36], i.e.,

$$\sum_{n=1}^{K}|\Delta\Psi(n)|^2 = \frac{1}{K}\sum_{i=1}^{K}\varepsilon_i^2, \tag{49}$$

Therefore, the energy of the phase noises is evenly projected onto each spectrum, indicating that the noise energy contaminating the DOA estimation is inversely proportional to the total number of sampling elements, because only one coefficient for a CA and two coefficients for an SA are involved in the DOA estimation. As a result, element number enhancement can alleviate the effect of phase noises upon spectrum calculations, consequently giving higher estimation accuracy. The following two sections will elaborate the accuracies of CAs and SAs in the spectral domain.

5.4. Estimation Accuracy of CA

Derivative of Eq. (16) gives

$$d\Psi_{CA}(1) = \pi k \rho_0 \left(e^{j\varphi_s} \cos\theta_s d\theta_s + j\sin\theta_s e^{j\varphi_s} d\varphi_s \right). \tag{50}$$

First-order approximation of Eq. (50) yields

$$\Delta\Psi_{CA}(1) = \pi k \rho_0 \left(e^{j\varphi_s} \cos\theta_s \Delta\theta_s + j\sin\theta_s e^{j\varphi_s} \Delta\varphi_s \right). \tag{51}$$

Comparison of real and imaginary parts of Eq. (50) with Eq. (51) leads to

$$\Delta\theta_s = \frac{2}{k\rho_0 \cos\theta_s} \left(\cos\varphi_s \sum_{i=1}^{N} \varepsilon_i \cos\varphi_i + \sin\varphi_s \sum_{i=1}^{N} \varepsilon_i \sin\varphi_i \right), \tag{52}$$

$$\Delta\varphi_s = \frac{2}{k\rho_0 \sin\theta_s} \left(\cos\varphi_s \sum_{i=1}^{N} \varepsilon_i \sin\varphi_i - \sin\varphi_s \sum_{i=1}^{N} \varepsilon_i \cos\varphi_i \right). \tag{53}$$

Taking Eq. (39) into Eqs. (52) and (53), respectively, we get the mean and variance of 2-D DOA estimations of an N-element CA, namely

$$\text{mean}(\Delta\theta_s) = 0, \tag{54}$$

$$\text{mean}(\Delta\varphi_s) = 0, \tag{55}$$

$$\text{var}(\Delta\theta_s) = 2\sigma^2 (k\rho_0 \cos\theta_s)^{-2}/N, \tag{56}$$

$$\text{var}(\Delta\varphi_s) = 2\sigma^2 (k\rho_0 \sin\theta_s)^{-2}/N. \tag{57}$$

Equations (54) and (55) suggest that applications of SDIE to DOA estimations are unbiased. Also, as shown in Eqs. (56) and (57), the variances of angle estimations by a CA are independent of the azimuth angle φ_s, which agrees with the rotation invariance of CAs.

5.5. Estimation Accuracy of SA

First-order approximation of derivative of Eq. (21) gives

$$\Delta\Psi_{SA}(1,1) = 2\pi k r_0 \left(e^{j\varphi_s} \cos\theta_s \Delta\theta_s + j\sin\theta_s e^{j\varphi_s} \Delta\varphi_s \right)/3. \tag{58}$$

Taking Eq. (48) into Eq. (58) leads to

$$\Delta\varphi_s = \frac{2}{2\pi k r_0/3} \left(Q\cos\varphi_s - P\sin\varphi_s \right). \tag{59}$$

where $P = \sum_{l=1}^{M} \sum_{i=1}^{N} \varepsilon_{il} \sin\theta_l \cos\varphi_i$ and $Q = \sum_{l=1}^{M} \sum_{i=1}^{N} \varepsilon_{il} \sin\theta_l \sin\varphi_i$. Hence, comparing real and imaginary parts of Eqs. (58) and (59), we get the mean and variance of the azimuth angle by a SA, namely

$$\text{mean}(\Delta\varphi_s) = 0, \tag{60}$$

$$\text{var}(\Delta\varphi_s) = 4\sigma^2 (k r_0 \sin\theta_s)^{-2}/(MN). \tag{61}$$

First-order approximation of derivative of Eqs. (20) and (21) gives

$$\Delta\theta_s = \frac{2\Delta|\Psi_{SA}(1,1)|\cos\theta_s - \Delta\Psi_{SA}(0,1)\sin\theta_s}{|\Delta\Psi_{SA}(0,1) + 2j\Delta|\Psi_{SA}(1,1)||}, \tag{62}$$

Meanwhile, first-order approximation of derivative of the magnitude of $\Psi_{SA}(1,1)$ also gives

$$\Delta\left|\Psi_{SA}(1,1)\right| = 2\pi kr_0 \sin\theta_s \left(P\cos\theta_s + Q\sin\theta_s\right) \bigg/ \left(3\left|\Psi_{SA}(1,1)\right|\right). \tag{63}$$

Considering $\Delta\Psi_{SA}(1,0) = \sum_{l=1}^{M}\sum_{i=1}^{N}\varepsilon_{il}\cos\theta_l$, then we have

$$\text{mean}\left(\Delta\theta_s\right) = 0, \tag{64}$$

$$\text{var}\left(\Delta\theta_s\right) = 4\sigma^2\left(kr_0\right)^{-2}\left(1+\sin^2\theta_s\right)^{-1}\bigg/(MN). \tag{65}$$

Equations (60) and (64) suggest unbiased estimations of the SDIE for SAs, while Eqs. (61) and (65) indicate that the estimation accuracies are inversely proportional to the number of sampling elements. Comparison of the results in Section 5.2 with Section 5.4 and Section 5.5 reveals that the lower bounds are attained, and hence the SDIE realizes an optimal estimation.

6. SIMULATION RESULTS

A CA and an SA were employed for simulations, respectively. The elevation angle was varied from 0 degree to 90 degrees, and the azimuth angle was fixed at 70 degrees. Phase noises were considered as independent AWGN with covariance of $(5°)^2$. Two uniform CAs with radius $\rho_0 = \lambda$ and element
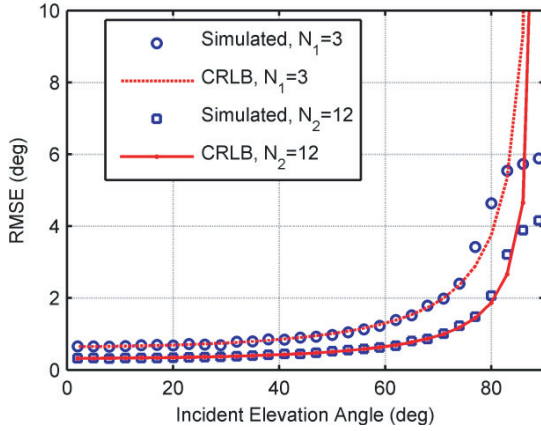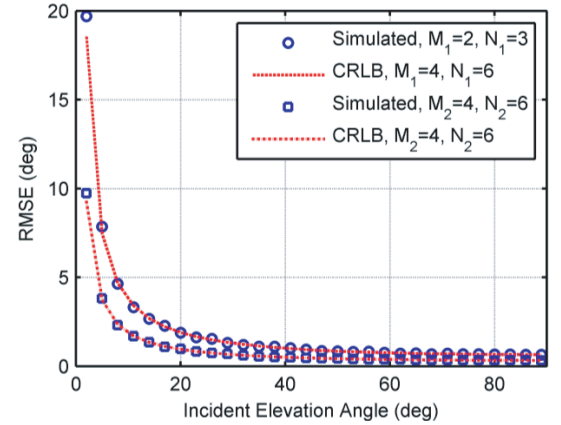

Figure 3. RMSEs of elevation angle estimation by a CA.
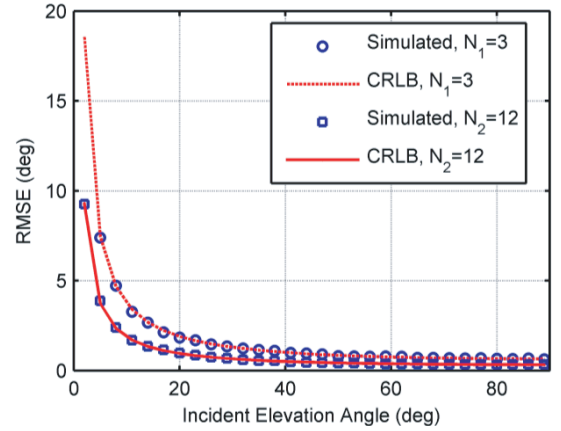
Figure 4. RMSEs of azimuth angle estimation by a CA.
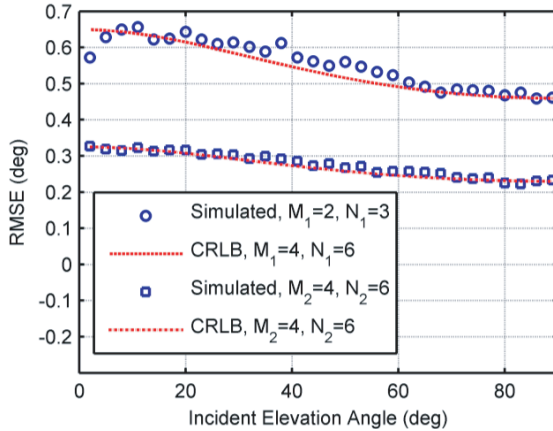
Figure 5. RMSEs of elevation angle estimation by a SA.

Figure 6. RMSEs of azimuth angle estimation by a SA.

number $N_1 = 3$ and $N_2 = 12$ were first exemplified. One thousand Monte Carlo simulations were run to estimate 2-D DOAs by Eqs. (27) and (28). Root mean square errors (RMSEs) of elevation and azimuth angles are shown in Fig. 3 and Fig. 4, respectively. As shown in Fig. 3 and Fig. 4, the simulated results approach the CRLB, indicating that the optimal estimation is achieved. The ratio of RMSE by $N_1 = 3$ to that by $N_2 = 12$ is 2, which equals $\sqrt{N_2/N_1}$ in this example. It is also noted that the RMSE rises as the elevation angle increases.

In the second simulation, we investigated the performance of SAs. The radius was $r_0 = \lambda$, and the numbers of elements were chosen as the minimum number, i.e., $M_1 = 2$ and $N_1 = 3$, as well as $M_2 = 4$ and $N_2 = 6$ for comparison. RMSEs of elevation and azimuth angles were calculated via one thousand Monte Carlo simulations, shown in Fig. 5 and Fig. 6, respectively. In Fig. 5, it is clearly seen that the accuracy dependence on the elevation angle is alleviated. In Fig. 6, the RMSE of azimuth estimation also agrees with the CRLB. It can also be seen that 4 times of element number give an accuracy enhancement by a factor of 2.

7. MEASUREMENT RESULTS

To verify the effectiveness of the proposed algorithm, a CA consisting of 15 log periodic dipole antennas was utilized for measurement in a microwave anechoic chamber. The radius of the measured CA was 1.5 m, as illustrated in Fig. 7. The CA was placed on a rotator, scanning the incident angle horizontally from −60 degrees to 60 degrees. The operating frequency was 1.8 GHz. A network analyzer was used to measure the phase of each antenna element. The SNR is 30 dB, and the phase measurement noises arose
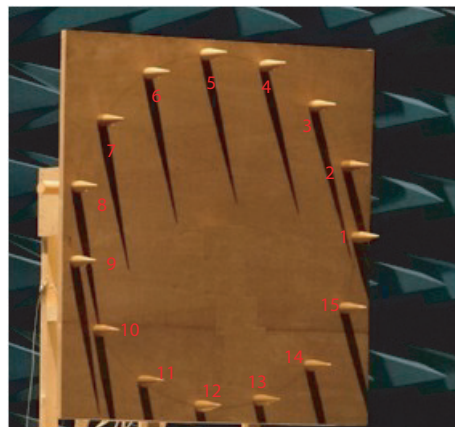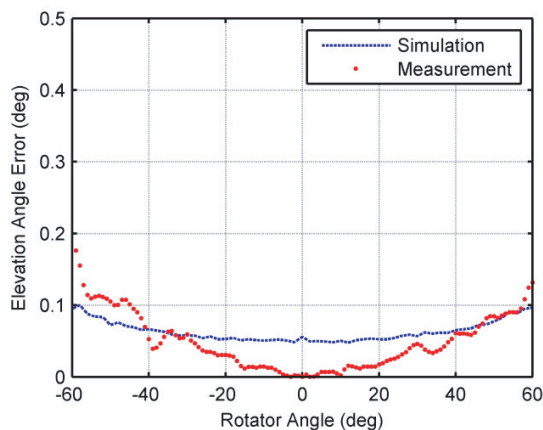

Figure 7. Measured UCA.

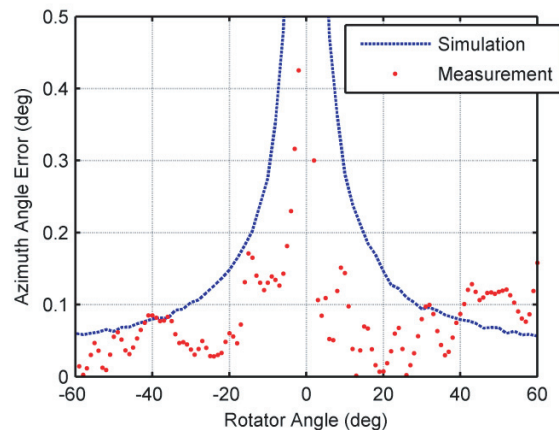**Figure 8.** Elevation angle error.

Figure 9. Azimuth angle error.

mainly from hardware imperfections. The standard deviation of phases of the antennas is 10 degrees. The simulated and measured elevation and azimuth angle estimation errors are shown in Fig. 8 and Fig. 9, respectively. As seen from Fig. 8 and Fig. 9, the accuracy of elevation angle estimation is higher than 0.2 degrees, and the accuracy of azimuth angle estimation is higher than 0.5 degrees.

8. CONCLUSIONS

This paper has proposed the SDIE through integral transforms, and two DOA estimation algorithms for CA and SA interferometers based on it. SDIEs for planar arrays, SAs and CAs have been established. The underlying DOA estimation problem has been reformulated as an equivalent expansion coefficient extraction problem by discrete phase samples. DOAs have been estimated in the spectrums of spatial phase distribution. Elevation and azimuth angles have been decoupled and calculated by analytical and accurate formulae relevant to discrete phase data. Accuracy analysis of the proposed method has demonstrated that it attains the CRLB, and hence it is an optimal estimation. Furthermore, Parseval's theorem has enabled us to show that larger number of sampling elements gives higher DOA estimation accuracy. Analysis and numerical examples have also provided mathematical insights into advantages in DOA estimation accuracy using the SDIE. Finally, a CA consisting of 15 antennas has been measured to verify the proposed method.

REFERENCES

1. Wu, Y. and H. C. So, "Simple and accurate two-dimensional angle estimation for a single source with uniform circular array," *IEEE Antennas Wireless Propag. Lett.*, Vol. 7, 78–80, 2008.
2. Wu, Y. W., S. Rhodes, and E. H. Satorius, "Direction of arrival estimation via extended phase interferometry," *IEEE Trans. Aerosp. Electron. Syst.*, Vol. 31, No. 1, 375–381, 1995.
3. Seidman, L. P., "Bearing estimation error with a linear array," *IEEE Trans. Audio & Electroacoust.*, Vol. 19, No. 2, 147–157, 1971.
4. Jackson, B. R., S. Rajan, and B. J. Liao, "Direction of arrival estimation using directive antennas in uniform circular arrays," *IEEE Trans. Antennas Propag.*, Vol. 63, No. 2, 736–747, 2015.
5. Pace, P. E., D. Wickersham, D. C. Jenn, and N. S. York, "High-resolution phase sampled interferometry using symmetrical number systems," *IEEE Trans. Antennas Propag.*, Vol. 49, No. 10, 1411–1423, 2001.
6. Lee, J. H. and J. M. Woo, "Interferometer direction-finding system with improved DF accuracy using two different array configurations," *IEEE Antennas Wireless Propag. Lett.*, Vol. 14, 719–722, 2015.
7. Liu, Z. M., Z. T. Huang, and Y. Y. Zhou, "Computationally efficient direction finding using uniform linear arrays," *IET Radar, Sonar, Navigation*, Vol. 6, No. 1, 39–48, 2012.
8. Liang, J. and D. Liu, "Two L-shaped array-based 2-D DOAs estimation in the presence of mutual coupling," *Progress In Electromagnetics Research*, Vol. 112, 273–298, 2011.
9. Liao, B., Y. T. Wu, and S. C. Chan, "A generalized algorithm for fast two-dimensional angle estimation of a single source with uniform circular arrays," *IEEE Antennas Wireless Propag. Lett.*, Vol. 11, No. 2, 984–986, 2012.
10. Ioannides, P. and C. A. Balanis, "Uniform circular arrays for smart antennas," *IEEE Antennas Propag. Magazine*, Vol. 47, No. 4, 192–206, 2005.
11. Mathews, C. P. and M. D. Zoltowski, "Eigenstructure techniques for 2-D angle estimation with uniform circular array," *IEEE Trans. Signal Process.*, Vol. 42, No. 9, 2395–2407, 1994.
12. Yang, P., F. Yang, and Z.-P. Nie, "DOA estimation with sub-array divided technique and interporlated ESPRIT algorithm on a cylindrical conformal array antenna," *Progress In Electromagnetics Research*, Vol. 103, 201–216, 2010.
13. Si, W., L. Wan, L. Liu, and Z. Tian, "Fast estimation of frequency and 2-D DOAs for cylindrical conformal array antenna using state-space and propagator method," *Progress In Electromagnetics Research*, Vol. 137, 51–71, 2013.

14. Belloni, F. and V. Koivunen, "Beamspace transform for UCA: Error analysis and bias reduction," *IEEE Trans. Signal Process.*, Vol. 54, No. 8, 3078–3089, 2006.

15. Huang, Q., L. Zhang, and Y. Fang, "Two-stage decoupled DOA estimation based on real spherical harmonics for spherical arrays," *IEEE/ACM Trans. Audio Speech Lang. Process.*, Vol. 25, No. 11, 2045–2058, 2017.

16. Teutsch, H., *Modal Array Signal Processing: Principles and Applications of Acoustic Wavefield Decomposition (Lecture Notes in Control and Information Sciences)*, Springer, Berlin, Germany, 2007.

17. De Witte, E., H. Griffith, and P. Brennan, "Phase mode processing for spherical arrays," *Electron. Lett.*, Vol. 39, No. 20, 1430–1431, 2003.

18. Meyer, J. and G. Elko, "A highly scalable spherical microphone array based on an orthonormal decomposition of the soundfield," *Proc. IEEE Int. Conf. Acoust., Speech, Signal Process.*, Vol. 2, 1781–1784, May 2002.

19. Rafaely, B., "Analysis and design of spherical microphone arrays," *IEEE Trans. Speech Audio Process.*, Vol. 13, 135–143, 2005.

20. Rafaely, B., "The spherical-shell microphone array," *IEEE Trans. Audio, Speech, Lang. Process.*, Vol. 16, No. 4, 740–747, 2008.

21. Rafaely, B., *Fundamentals of Spherical Array Processing, (Springer Topics in Signal Processing)*, Springer-Verlag, Berlin, Germany, 2015.

22. Rafaely, B., "Plane-wave decomposition of the pressure on a sphere by spherical convolution," *J. Acoust. Soc. Amer.*, Vol. 116, 2149–2157, 2004.

23. Moore, A., C. Evers, and P. Naylor, "Direction of arrival estimation in the spherical harmonic domain using subspace pseudo-intensity vectors," *IEEE/ACM Trans. Audio Speech Lang. Process.*, Vol. 25, No. 1, 178–192, 2017.

24. Costa, M., A. Richter, and V. Koivunen, "Unified array manifold decomposition based on spherical harmonics and 2-D Fourier basis," *IEEE Trans. Signal Process.*, Vol. 58, No. 9, 4634–4645, 2010.

25. Goossens, R. and H. Rogier, "Unitary spherical ESPRIT: 2-D angle estimation with spherical arrays for scalar fields," *IET Signal Process.*, Vol. 3, No. 3, 221–231, 2008.

26. Goossens, R. and H. Rogier, "A hybrid UCA-RARE/Root-MUSIC approach for 2-D direction of arrival estimation in uniform circular arrays in the presence of mutual coupling," *IEEE Trans. Antennas Propag.*, Vol. 55, No. 3, 841–849, 2007.

27. Wang, B. H., H. T. Hui, and M. S. Leong, "Decoupled 2D direction of arrival estimation using compact uniform circular arrays in the presence of elevation-dependent mutual coupling," *IEEE Trans. Antennas Propag.*, Vol. 58, No. 3, 747–755, 2010.

28. Harrington, R. F., *Time-harmonic Electromagnetic Fields*, McGraw-Hill, 2001.

29. Driscoll, J. R. and D. M. Healy, Jr., "Computing Fourier transforms and convolutions on the 2-sphere," *Adv. Appl. Math.*, Vol. 15, No. 2, 202–250, 1994.

30. Williams, E. G., *Fourier Acoustics: Sound Radiation and Nearfield Acoustical Holography*, 1st Edition, Academic, London, U.K., 1999.

31. Kay, S. M., "A fast and accurate single frequency estimator," *IEEE Trans. Acoustics, Speech, Signal Process.*, Vol. 37, No. 12, 1987–1990, 1989.

32. Tretter, S. A., "Estimating the frequency of a noisy sinusoid by linear regression," *IEEE Trans. Inf. Theory*, Vol. 31, No. 6, 832–835, 1985.

33. Rife, D. and R. Boorstyn, "Single tone parameter estimation from discrete-time observations," *IEEE Trans. Inf. Theory*, Vol. 20, No. 5, 591–598, 1974.

34. Mcaulay, R., "Interferometer design for elevation angle estimation," *IEEE Trans. Aerosp. Electron. Syst.*, Vol. 13, No. 5, 486–503, 1977.

35. Kay, S. M., *Fundamentals of Statistical Signal Processing: Estimation Theory*, PTR Prentice Hall, 1993.

36. Robert, J. M., II, *Handbook of Fourier Analysis and Its Applications*, Oxford University Press, 2009.